AAS 19-220

# ANALYZING FEASIBILITY OF OPTICAL COMMUNICATION OBSERVABLES FOR NAVIGATION

**Sarah Elizabeth McCandless*and Tomas J. Martin-Mur†**

Future deep-space missions are intending to utilize optical communications and thereby take advantage of superior data delivery rates. The same laser-based links could also be used for interplanetary navigation. Two main optical tracking types could be used for this purpose. The first is optical ranging that uses active optical systems at both ends of the link, as opposed to passive systems. The second is optical astrometry, where a telescope images the spacecraft laser against a star background and thereby resolves plane-of-sky position. These data types offer similar capabilities to the radiometric techniques used for current interplanetary missions. These missions have a variety of objectives and requirements, which impacts trajectory determination and the necessary data types. This paper discusses the formulation of the data types and their success in meeting mission requirements for two mission scenarios: a network of spacecraft in orbit about Mars and a spacecraft in a halo orbit at the Earth-Sun L1 Lagrange point.

## NOMENCLATURE

| | |
|---|---|
| $T$ | = Time |
| $D$ | = Telescope diameter |
| $a, b$ | = Optical measurement uncertainty coefficients |
| $MRO$ | = Mars Reconnaissance Orbiter |
| $NEOCam$ | = Near-Earth Object Camera |
| $LOS$ | = Line-of-sight |

## INTRODUCTION

NASA is turning to laser communications for future deep-space missions. A first-generation optical communications terminal[1] will be flown on Pysche, the next Discovery mission, in 2022.[2] This new technology enables larger and faster scientific data transfer from deep-space, which is increasingly important as the world continues to send more missions to space. With some adaptations, the same equipment used for optical communication could be used for trajectory determination. Previous missions have conducted laser ranging experiments, but none of the systems were sufficient to replace radiometric tracking systems. The Mercury Laser Altimeter on MESSENGER[3],[4] the Lunar Orbiter Laser Alitmeter (LOLA) on the Lunar Reconnaissance Orbiter (LRO),[5] and the

*Navigation Engineer, NASA Jet Propulsion Laboratory, California Institute of Technology, 4800 Oak Grove Drive, Pasadena, CA 91109

†Supervisor, Inner Planet Navigation Group, NASA Jet Propulsion Laboratory, California Institute of Technology, 4800 Oak Grove Drive, Pasadena, CA 91109

Lunar Laser Communications Demonstration on the Lunar Atmosphere Dust Environment Explorer (LADEE)[6] are some of these missions. Future optical systems must be capable over interplanetary distances and use active links. The optical communication observables of interest are optical range and optical astrometry. Optical range data simulated for this analysis uses an active system at each end of the link, and accuracies from a few millimeters to a few centimeters should be possible.[7] Optical astrometry data will be vastly improved by the release of the star catalog from the European Space Agency's (ESA) Gaia mission.[8] Combined with advances in observing techniques and instrumentation, accuracies to the nanoradian level should be possible.[9]

In assessing the performance of optical communication observables, thorough measurement models, geometrical constraints, and tracking schedules are simulated and analyzed. Different mission scenarios also have varying requirements that impact the trajectory determination. Mars lander missions, for example, have much tighter constraints than an interplanetary orbiter. The analyses presented here include a network of spacecraft in orbit at Mars and a near-Earth science mission. The Martian network of spacecraft is comprised of two cubesats in differing altitude circular orbits and a telecommunications orbiter. The near-Earth science mission is modeled after the Near-Earth Object Camera (NEOCam) mission, set to search for potentially hazardous asteroids.

## OPTICAL MEASUREMENT MODELS

Measurement simulation, filtering, and mapping is performed using Mission Analysis, Operations, and Navigation Toolkit Environment (MONTE), a JPL multi-purpose software that supports the design and analysis of deep space missions.[10] Compared to their radiometric counterparts, optical measurements have the distinct advantage of not being impacted by charged particles and the disadvantage of being susceptible to local weather. That optical frequencies are not impacted by charged particles negates the impact of solar plasma and the ionsphere, which improves light-time calculation and noise. Conversely, cloud cover, fog, or dust could completely prohibit transmission of optical signals, where they would just increase the noise of radio tracking data.

### Optical Space-Based Astrometry

While range measurements provide a distance measure to a spacecraft, angular measurements locate a spacecraft in the plane-of-sky. Traditional plane-of-sky measurements are created by calculating the difference in arrival time of one signal at two ground sites. The advantage of optical astrometry is that an active signal on a spacecraft can be imaged against background optical sources to determine the plane-of-sky measurement. In this way, the target and comparable sources are in the same images and errors introduced by tying the two together (which is done for radio measurements as they are compared against quasars) are negated.

Past studies[11,12,13] have demonstrated the effectiveness of ground-based astrometry. In these studies, a ground-based telescope images both the spacecraft and background optical sources. This study investigates the feasibility of space-based astrometry; here, the telescopes are mounted on the spacecraft themselves. In the Mars network of satellites scenario described in the following section, each cubesat in the network has an onboard telescope that takes the images that are then converted into angular measurement information. The measurement models are the same as those used in past ground-based astrometry studies, but the uncertainty of the space-based angular measurements is different from ground-based measurements. The analyses presented here use one-way right ascension and declination measurement models. It is assumed a team will process the optical images and provide the angular measurements to the spacecraft navigation team. The measurements are not

concerned with the Earth's atmosphere, so the following equations are used to determine the angular measurement uncertainty. T is integration time (e.g. average period) and D is telescope diameter.

$$\epsilon^2 = a + b \tag{1}$$

$$a \sim 0.75 \left(\frac{1\text{ m}}{D}\right)^2 \left(\frac{1\text{ hour}}{T}\right) \text{mas}^2, b \sim 0.25 \left(\frac{1\text{ m}}{D}\right)^2 \left(\frac{1\text{ hour}}{T}\right) \text{mas}^2 \tag{2}$$

### Optical Range

Ranging measurements record the round-trip light-time of a signal and are feasible at optical frequencies. Across deep-space distances, however, simple retroreflectors are not sufficient. An active system is necessary onboard the spacecraft, and it would track the uplink signal and generate the downlink signal necessary to transmit the appropriate ranging data. The measurement model for optical ranging is the same as that for radio ranging, excluding the ionospheric group delay. Both simulations discussed here assume two-way optical range measurements, though one-way measurements could be possible if high-precision atomic clocks are available at each end of the link.

## MARS NETWORK OF SATELLITES

One of the cases analyzed in this report models a network of cubesats in orbit about Mars. One 14 kg cubesat is in a 400 km circular orbit about Mars, and the second is in a 4000 km orbit. The orbital planes are orthogonal to each other. Each cubesat is equipped with the optical communications hardware necessary for optical tracking. Additionally, a telecommunications orbiter (modeled after the Mars Reconnaissance Orbiter, MRO) is included in the network. Like the cubesats, this orbiter is also equipped with optical communications hardware and can optically track each cubesat. The larger telecommunications orbiter is assumed to have a more precisely known orbit, which is useful in determining the relative states of the cubesats. No radiometric tracking is simulated in this analysis. Figure 1 illustrates the network geometry.

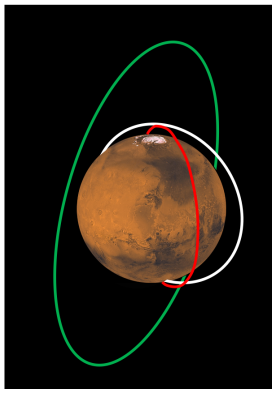

**Figure 1. Network Geometry. The MRO-like telecomm orbiter is in red, the low-altitude cubesat in white, and the high-altitude cubesat in green.**

This analysis case includes the impacts of solar radiation pressure and atmospheric density on the accuracy of the position determination. Both are modeled as stochastic parameters (their values are modeled after MRO). Additionally, desaturation burns are modeled as impulse burns once a day. Desaturation burns occur when reaction wheels (used to maintain attitude) become saturated and are no longer effective. De-spinning these wheels induces a small change in velocity to the spacecraft. Uncertainty in the orbits of both the telecommunications orbiter and the higher altitude cubesat is also considered. All orbit determination assumptions are summarized in Table 1. Additionally, all available contacts between spacecraft are used for navigation.

**Table 1. Mars Network Orbit Determination Error Assumptions**

| **Error Source** | **Estimate or Consider** | **A Priori Uncertainty ($1\sigma$)** |
|---|---|---|
| Telecommunications Orbiter State | Consider | 7.5 m, 2.4 mm/sec |
| High-altitude Cubesat State | Consider | 100 km, 10 m/s |
| Desaturation burns | Estimate | 0.3 mm/s per axis |
| Solar Radiation Pressure | Estimate | 0.3 |
| Atmospheric Density | Estimate | 0.6 |

This analysis case spans three days, February 28, 2015 5:50 ET to March 3, 2015 5:50 ET. Three desaturation burns occur: February 28, March 1, and March 2 at 11:50 ET each day. During that time, it is assumed that any valid link among any two spacecraft in the network is used for navigation. Additional constraints beyond a spacecraft being in view is a $30^\circ$ Sun exclusion angle as well as a Mars exclusion angle based on the assumption that the radius of Mars is 3396 km and it has a 200 km thick atmosphere. With these constraints in place, the following tracking schedules result; Figure 2 shows the astrometric tracking data and Figure 3 shows the range tracking data. For this analysis case, each measurement type is studied individually.

### Astrometry

The baseline scenario for the astrometry simulation makes the following assumptions: a five cm telescope diameter, a ten second integration time, a one minute sampling time, and that all contacts with the telecommunications orbiter are used. This results in astrometric uncertainties of approximately 0.5 arcsec. A sensitivity analysis is also performed, and each parameter (telescope diameter, integration time, sample time, and orbiter contacts) is studied to assess its impact on the orbit determination. These analyses are shown in Figure 4 and Figure 5 and summarized in Table 2 and Table 3. In each figure, the LOS plot refers to line-of-sight uncerainty, while the 3D plot refers to the total uncertainty. Figure 4 shows the state uncertainty of the target low-altitude cubesat relative to the higher-altitude cubesat, while Figure 5 shows the state uncertainty relative to the center of Mars. This latter case is illustrative of a scenario where a target point is well known and that can be used to tie down a less well-known spacecraft state. In both figures, the short-term signature is due to the tracking data schedule. A forward filter is used, and the uncertainty decreases as time increases. In operations, multiple arcs would be strung together such that this higher initial uncertainty would be overwritten.

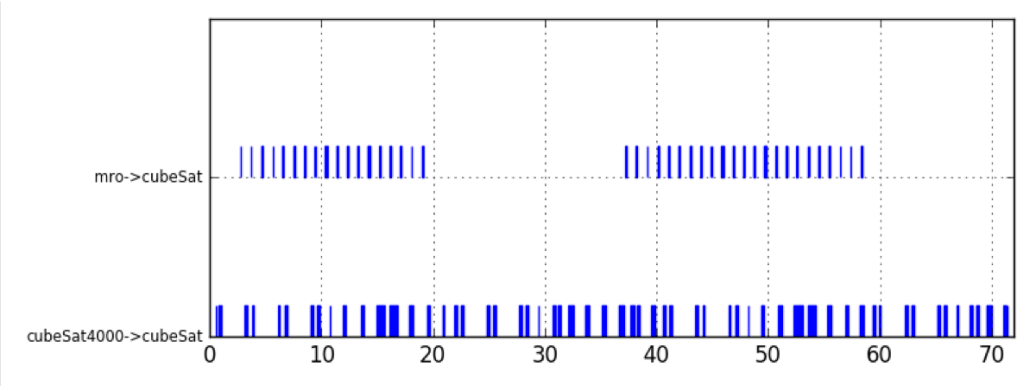


**Figure 2. Astrometric tracking schedule. The top row shows contacts between the MRO-like telecommunications orbiter and the low-altitude cubesat; the bottom shows contacts between the two cubesats. The x-axis shows the number of hours from the beginning of the simulation.**

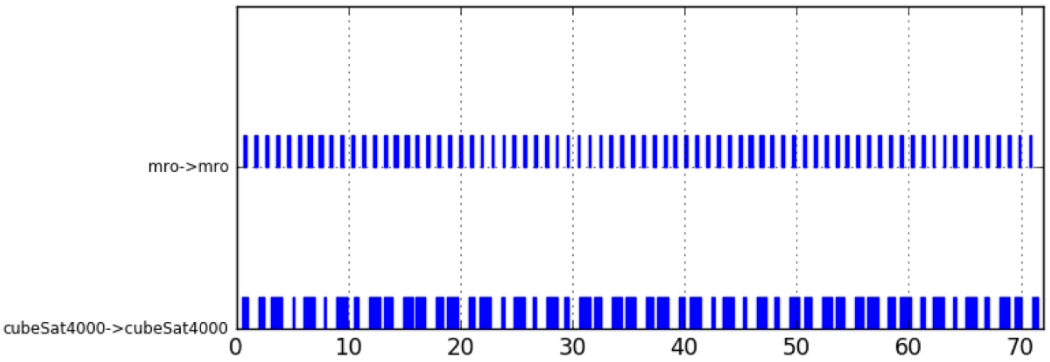


**Figure 3. Optical range tracking schedule. The top row shows contacts between the MRO-like telecommunications orbiter and the low-altitude cubesat; the bottom shows contacts between the two cubesats. The x-axis shows the number of hours from the beginning of the simulation.**

Enlarging the telescope diameter reduces the astrometric measurement uncertainty and improves the results slightly, but a 20 cm diameter is the likely limit for a spacecraft as small as a cubesat. Larger diameters would likely create more operational burdens than the performance improvements they would offer. Both figures also demonstrate the state sensitivity to sample time. Additionally, the desaturation burns introduce state errors, but these are not significant (see Table 3). The geometry offers enough contact between the two cubesats that eliminating the contact with the telecommunications orbiter is not catastrophic. While the initial position uncertainty is degraded, there is enough inter-cubesat tracking data to recover. As evidenced by these analyses, astrometric data types allow for absolute position determination even when no other data types are used.

### Optical Range

The baseline scenario for the optical range simulation makes the following assumptions: five cm uncertainty, ten second integration time, one minute sampling time, and that all telecommunications

**Figure 4. Relative state uncertainties of a low-altitude cubesat using astrometric measurements.**

orbiters contacts are being used. An additional case with the baseline parameters and desaturation burns modeled is also analyzed. Like the astrometry simulations, a sensitivity analysis is performed where each parameter's impact on the orbit determination is studied. These analyses are shown in the Figure 6 and Figure 7 below and summarized in Table 2 and Table 3. In each figure, the LOS plot refers to line-of-sight uncerainty, while the 3D plot refers to the total uncertainty. Figure 6 shows the state uncertainty of the target low-altitude cubesat relative to the higher-altitude cubesat. Figure 7 shows the state uncertainty relative to the center of Mars. Like the astrometry cases, the short-term signature is due to the tracking data schedule.

As evidenced by these analyses, optical range measurements allow for position determination when the position of one spacecraft is well-known. Additionally, the telecommunications orbiter helps tie down non line-of-sight errors. Reducing the number of orbiter contacts degrades the uncertainty by an order of magnitude. This is different from the astrometry case, which is less sensitive to the orbiter. While the range measurements are more sensitive to orbiter contacts, they are less sensitive to desaturation burns. Also different from the astrometry case is the impact of sampling time on the range measurements. Initial position determination is degraded for less time, and the final position determination is only an order of magnitude worse as compared to five orders of magnitude for the astrometry simulations. This level of uncertainty is comparable to that achieved using dual one-way range rate measurements.

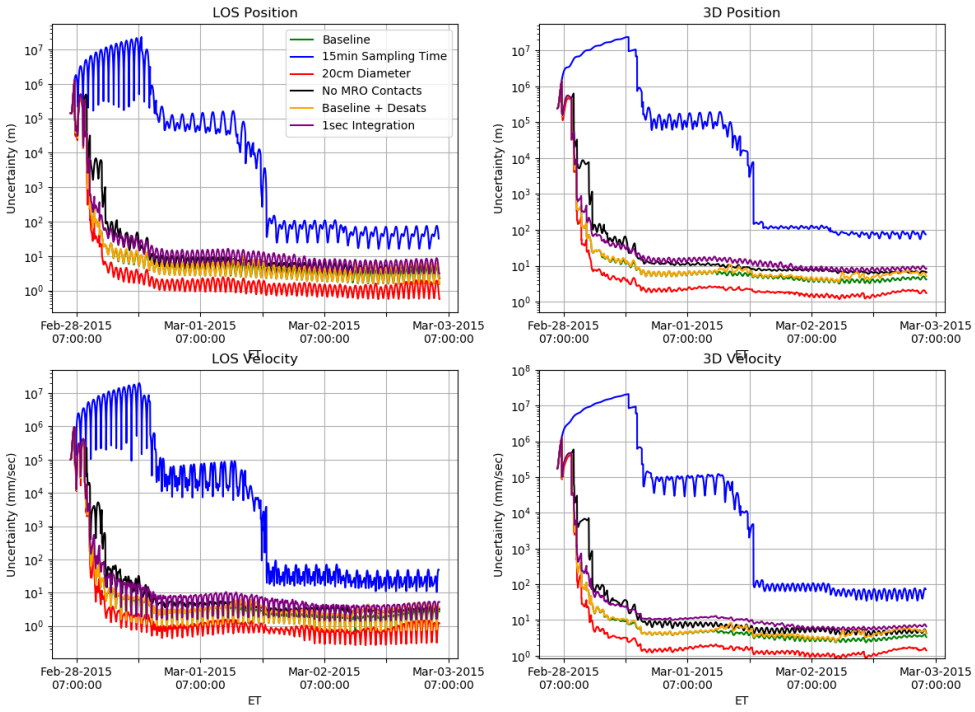


**Figure 5. Absolute state uncertainties of a low-altitude cubesat using astrometric measurements.**

Ultimately, these results show that optical measurement types are a viable alternative for this mission scenario. Performance is comparable to radio tracking, and previous research into the impact of orbital geometry found the orthogonal orbits to be the most restrictive. While exact geometries will impact the number of contacts among the spacecraft in the network, the results of this study should apply to any network geometry.

**Table 2. Baseline Cubesat State Uncertainties**

| | **LOS Velocity** | **3D Velocity** | **LOS Position** | **3D Position** |
|---|---|---|---|---|
| Relative Radio Range + Doppler | 0.050 mm/s | 0.26 mm/s | 92 mm | 28 cm |
| Relative Astrometry | 2.4 mm/s | 6.7 mm/s | 2.8 m | 7.0 m |
| Absolute Astrometry | 2.3 mm/s | 3.9 mm/s | 3.9 m | 5.4 m |
| Relative Range | 0.052 mm/s | 2.9 mm/s | 5.3 cm | 2.9 m |
| Absolute Range | 0.59 mm/s | 1.3 mm/s | 67 cm | 1.5 m |

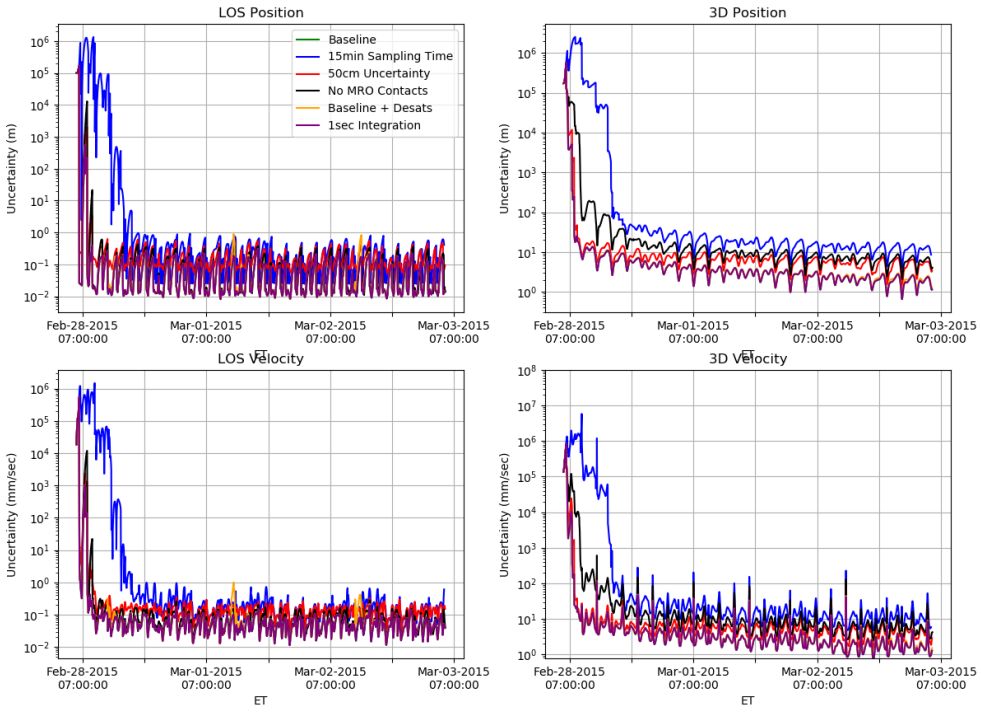


**Figure 6. Relative state uncertainties of a low-altitude cubesat using optical range measurements.**

**Table 3. Varying Cubesat Line-of-Sight Velocity Uncertainties**

| | Baseline | 15 Minute Sampling Time | 20 cm Diameter | 50 cm Uncertainty | No Orbiter Contacts | Baseline + Desats | 1 sec Integration |
|---|---|---|---|---|---|---|---|
| Relative Astrometry | 2.4 mm/s | 449 m/s | 0.91 mm/s | – | 4.2 mm/s | 2.8 mm/s | 5.9 mm/s |
| Absolute Astrometry | 2.3 mm/s | 520 m/s | 0.88 mm/s | – | 4.1 mm/s | 2.8 mm/s | 5.3 mm/s |
| Relative Range | 0.052 mm/s | 0.20 mm/s | – | 0.50 mm/s | 0.070 mm/s | 0.062 mm/s | 0.052 mm/s |
| Absolute Range | 0.59 mm/s | 2.9 mm/s | – | 1.1 mm/s | 1.6 mm/s | 0.62 mm/s | 0.59 mm/s |

## NEOCAM

The second case analyzed in this paper is a mission in a halo orbit at the Earth-Sun L1 Lagrange point. Near-Earth Object Camera (NEOCam) is a mission that aims to discover potentially hazardous near-Earth asteroids. It will use an infrared telescope and a wide-field camera operating at thermal infrared wavelengths to scan the sky for these objects. Operating in this wavelength allows NEOCam to more accurately measure asteroid size and shed light on asteroid composition, shape, and rotation. NEOCam will travel to the Earth-Sun L1 Lagrange point, placing it 1 million kilome-

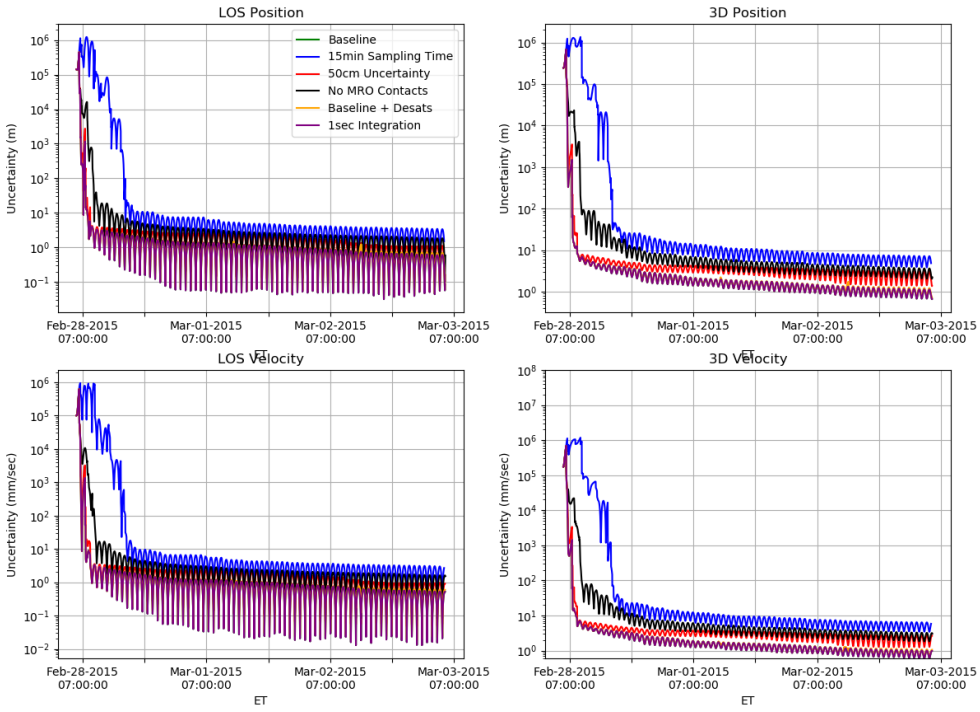


**Figure 7. Absolute state uncertainties of a low-altitude cubesat using optical range measurements.**

ters from Earth along the Earth-Sun line. Figure 8 illustrates this geometry. In this particular orbit, NEOCam will be able to scan a large portion of the space near Earth's orbit at one time. NEOCam is also equipped with a sunshade that allows it to survey for asteroids as close as 45° to the Sun. NEOCam has a four year primary mission, and during that time it is expected to identify two-thirds of the potentially hazardous asteroid population.

The simulation for this mission scenario models ground-based optical range measurements and space-based astrometric measurements based on NEOCam's science images. For the optical range measurements, a five minute sampling time and five cm uncertainty was assumed. The tracking schedule assumes five passes per week, each one hour in duration. Operationally, more passes may be scheduled, but five passes per week protects against lost passes (ground station outages, spacecraft safe-modes etc.). Due to its geometry, NEOCam is not a good candidate for ground-based astrometry. The optical images NEOCam takes for asteroid identification can also be used for position determination, however. This would be similar to traditional optical navigation, but unique because these images are not in the optical spectrum, and are instead in the infrared. These images would serve dual purpose as both science images and navigation images, and a team of individuals would process the images and determine the right ascension and declination of the asteroids. These measurements could then be used to determine the position of NEOCam itself.

This simulation creates angular measurements that mimic the right ascension and declination

measurements derived from the processed images. The first step in simulating these angular measurements is to determine which asteroids would be in the field of view of the camera aboard NEOCam. Asteroid set SB431-N343 contains the ephemerides of 343 small-body perturbers used to generate the DE431 ephemeris.[14] The subset of asteroids that are within the camera's field of view and are closest are used in this simulation. (The camera's field of view is 45° by 110° in the Sun elongation direction.[15]) This results in 167 unique asteroids being used over the duration of the simulation, which spans June 1, 2021 to January 31, 2022. Additional constraints on asteroid selection are that a unique asteroid may only be observed once every twelve days, and that the observation frequency of any asteroid is nine hours.[15] Asteroid position covariance was considered in the spacecraft position determination, and this covariance value was varied in the simulation. Traditional optical navigation has demonstrated that spacecraft state is sensitive to asteroid position covariance; the better we know the asteroids, the better we know the spacecraft state. Different asteroids have various covariances, but this study assumed a blanket value for each asteroid for simplicity. Current state-of-the-art position covariances are in the tens of kilometers, but future studies (including ESA's Gaia mission) could improve this. For this study, position covariance was set to 100 m, 1 km, 10 km, 50 km, 100 km, 1000 km, and 10,000 km. The uncertainty for the angular measurements was 0.5 arcsec.[15]

The performance achievable using radio range and doppler is shown in Figure 9. NEOCam mission requirements state the reconstructed spacecraft ephemeris must be known to $\pm$ 15 km per axis, $1\sigma$. As evidenced, that requirement is easily met. Figure 10 shows the performance achievable using ground-based optical range and astrometric measurements (assuming 50 km asteroid position covariance). Performance is comparable to that achieved with radiometric measurements; as seen in Table 4, it is actually slightly improved, and mission requirements are easily satisfied. When asteroid position covariance is inflated, the resulting performance is not degraded. The large uncertainty of the astrometric measurements negates the impact of considering the asteroid ephemeris. If, however, the uncertainty is tightened, asteroid position covariance plays a larger role. Additional sensitivity studies found that for an uncertainty of 4 milliarcsec (two orders of magnitude improvement in uncertainty), predicted spacecraft position begins to worsen for an asteroid position covariance of 50 km. If the covariance is set to 1000 km, mission requirements are no longer met. For this case, using poorly known asteroids is worse than using no astrometry data at all. Figure 11 demonstrates the performance achievable using only optical range, which is comparable to traditional radiometrics. For this particular mission scenario, then, optical range alone is sufficient. Even then, optical range does not offer significant improvements over traditional radio range and doppler. Additional studies did show a sensitivity to density of range measurements. If the number of passes per week is reduced from 5 to 3, performance is degraded, and the spacecraft is more sensitive to orbital geometry. This is shown in Figure 12. All results are summarized in Table 4.

## CONCLUSION

The analyses presented here demonstrate that optical tracking data types are a viable alternative to radiometric data types for the considered mission scenarios. For a network of spacecraft in orbit about Mars, astrometric measurements allow for absolute position determination even when no other measurement types are used. Range measurements allow for position determination when the position of one spacecraft is well-known, and a telecommunications orbiter (an optically equipped MRO, for example) aids in reducing non line-of-sight errors. For a mission at the Earth-Sun L1 point, astrometric measurements as used from the science images do not improve state knowledge,

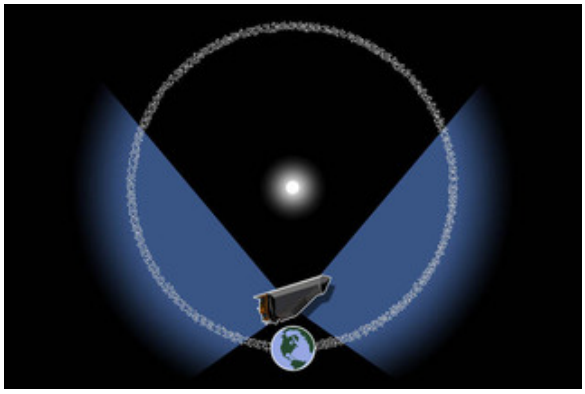

**Figure 8. NEOCam's Orbital Geometry.[16]**

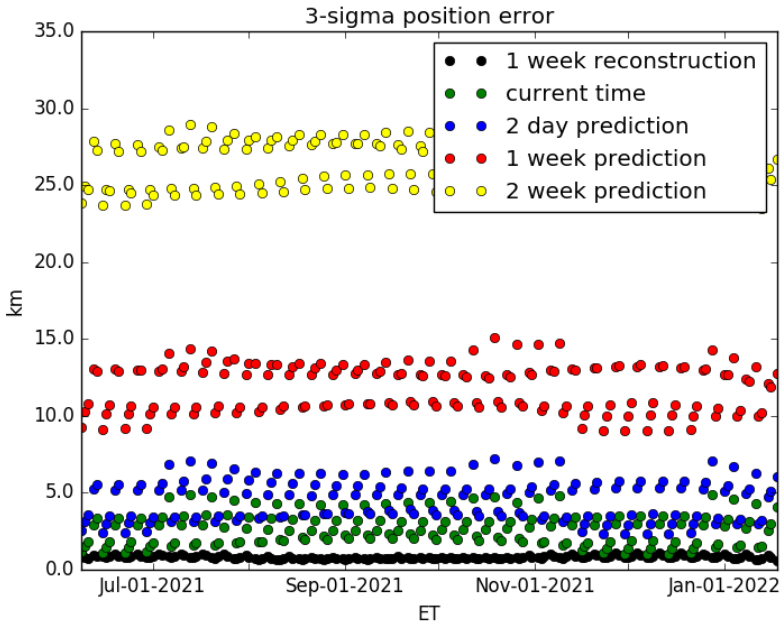


**Figure 9. NEOCam state uncertanties using radio range and doppler.**

and poor astrometric measurements can actually degrade it. Range measurements provide comparable state information, but the density of range measurements is important.

## ACKNOWLEDGEMENTS

The authors wish to thank Chengxing Zhai, Michael Shao, Todd Ely, Christopher Jacobs, Joseph Lazio, and Slava Turyshev for their help with this research.

The navigation work described in this paper was carried out at the Jet Propulsion Laboratory, California Institute of Technology, under a contract with the National Aeronautics and Space Ad-

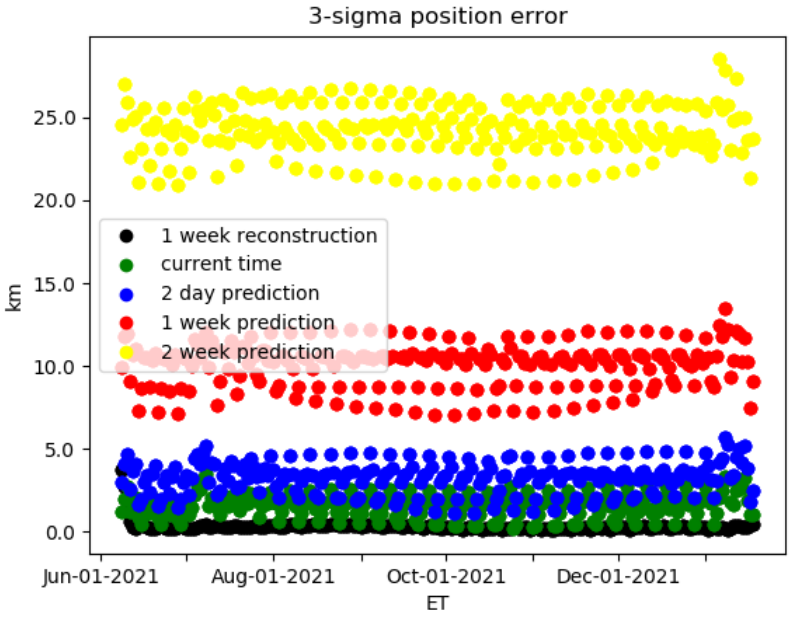


**Figure 10. NEOCam state uncertanties using optical range and astrometry. An asteroid position covariance of 50km is assumed.**

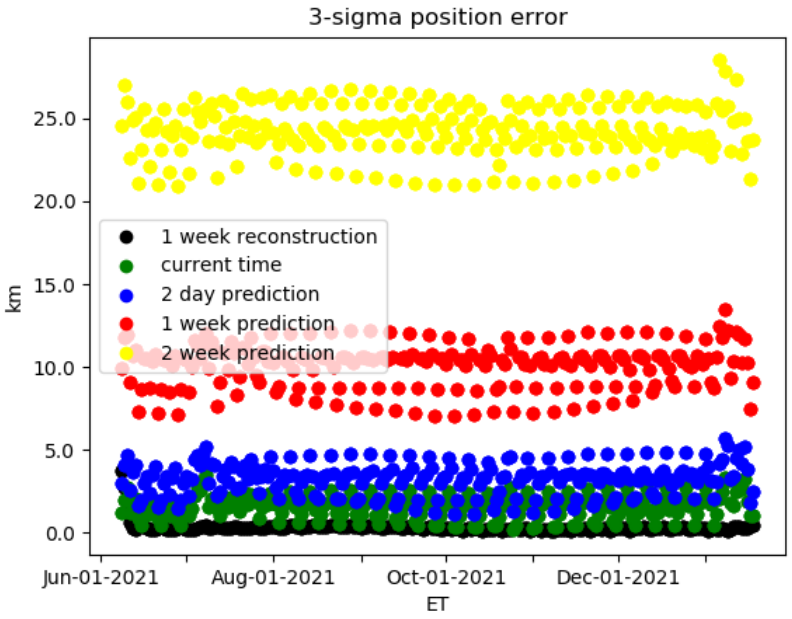


**Figure 11. NEOCam state uncertanties using optical range only.**

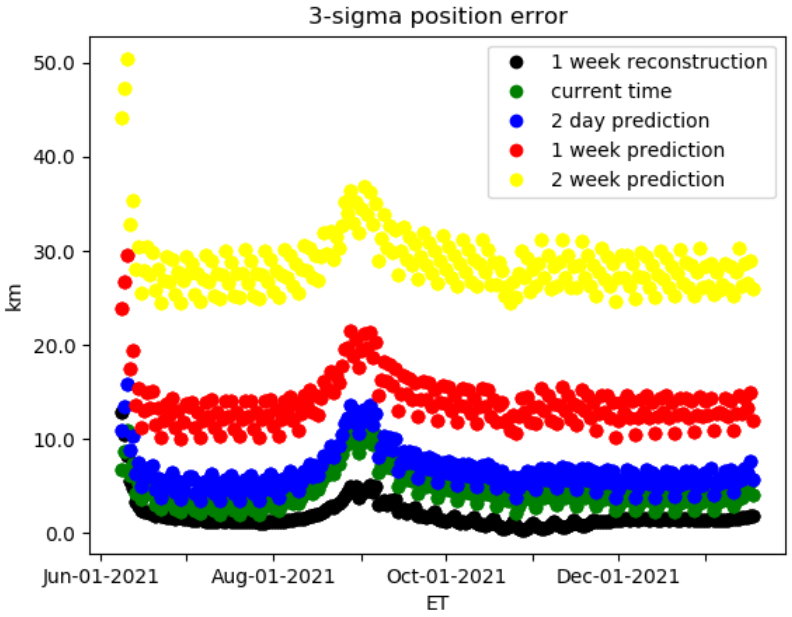


**Figure 12. NEOCam state uncertanties using optical range only. Pass density is decreased to three passes per week.**

**Table 4. NEOCam State Uncertainty Means**

| | **Radio Range + Doppler** | **Optical Range +Astrometry (50 km Asteroid Covariance)** | **Optical Range Only** | **Optical Range Only, 3 Passes/Wk** |
|---|---|---|---|---|
| 1 Week Reconstruction | 0.82 km | 0.31 km | 0.31 km | 1.8 km |
| Current Time | 2.6 km | 1.6 km | 1.6 km | 4.5 km |
| 2 Day Prediction | 4.6 km | 3.3 km | 3.3 km | 6.5 km |
| 1 Week Prediction | 11.8 km | 10.1 km | 10.1 km | 14.0 km |
| 2 Week Prediction | 26.3 km | 24.3 km | 24.3 km | 28.8 km |



## REFERENCES

[1] *Discovery deep space optical communications (DSOC) transceiver*, Vol. 10096, 2017, 10.1117/12.2256001.

[2] D. Oh *et al.*, "Development of the Psyche Mission for NASA's Discovery Program," *35th International Electric Propulsion Conference, Georgia Institute of Technology, Atlanta, Georgia*, IEPC-2017-153, October 2017.

[3] D. Smith *et al.*, "Two-Way Laser Link over Interplanetary Distance," *Science*, Vol. 311, 2006, p. 311.

[4] J. Cavanaugh *et al.*, "The Mercury Laser Altimeter instrument for the MESSENGER mission," *Space Sci. Rev.*, Vol. 131, 2007, pp. 451–480.

[5] M. Zuber *et al.*, "The Lunar Reconnaissance Orbiter Laser Ranging Investigation," *Space Sci. Rev.*, Vol. 150, 2010, pp. 63–80.

[6] D. M. Boroson, B. S. Robinson, D. V. Murphy, D. A. Burianek, F. Khatri, J. M. Kovalik, Z. Sodnik, and D. M. Cornwell, "Overview and results of the Lunar Laser Communication Demonstration," *Proc. SPIE*, Vol. 8971, 2014, pp. 89710S–89710S–11, 10.1117/12.2045508.

[7] W. M. Folkner *et al.*, "Preliminary Error Budget for an Optical Ranging System: Range, Range Rate, and Differenced Range Observables," tech. rep., TDA Progress Report 42-101, 121-135, 1990.

[8] T. Prusti *et al.*, "The Gaia Mission," *A&A 595, A1*, 2016.

[9] C. Zhai *et al.*, "Nanoradian ground-based astrometry, optical navigation, and artificial reference stars," *Proc. SPIE Astronomical Telescopes and Instrumentations*, 2016.

[10] S. Evans *et al.*, "MONTE: The Next Generation of Mission Design & Navigation Software," *The 6th International Conference on Astrodynamics Tools and Techniques (ICATT)*, 2016.

[11] S.-E. McCandless and T. Martin-Mur, "Navigation using deep-space optical communication systems," *AIAA/AAS Astrodynamics Specialit Conference, AIAA SPACE Forum*, 2016.

[12] T. Martin-Mur, S.-E. McCandless, and R. Karimi, "Deep-space navigation using optical communication systems," *26th International Symposium on Space Flight Dynamics, Matsuyama, Japan*, 2017.

[13] R. Karimi, T. Martin-Mur, and S.-E. McCandless, "A Performance Based Comparison of Deep-space Navigation using Optical Communication and Conventional Navigation Techniques: Small Body Missions," *Space Flight Mechanics Meeting, AIAA SciTech Forum*, 2018.

[14] D. Fanocchia, "Small-Body Perturber Files SB431-N16 and B432-N343," 2014.

[15] A. Mainzer, T. Grav, J. Bauer, T. Conrow, R. M. Cutri, J. Dailey, J. Fowler, J. Giorgini, T. Jarrett, J. Masiero, T. Spahr, T. Statler, and E. L. Wright, "Survey Simulations of a New Near-Earth Asteroid Detection System," *The Astronomical Journal*, Vol. 149, May 2015, p. 172, 10.1088/0004-6256/149/5/172.

[16] NASA/JPL-Caltech, "NEOCam's Viewing Geometry,"